Atomic Resolution Imaging at an Ultralow Accelerating Voltage by a Monochromatic Transmission Electron Microscope

Shigeyuki Morishita,[1,*] Masaki Mukai,[1] Kazu Suenaga,[2] and Hidetaka Sawada[1]
[1]JEOL Limited, 3-1-2 Musashino, Akishima, Tokyo 196-8558, Japan
[2]National Institute of Advanced Industrial Science and Technology (AIST), 1-1-1 Higashi, Tsukuba, Ibaraki 305-8565, Japan
(Received 20 June 2016; published 6 October 2016)

Transmission electron microscopy using low-energy electrons would be very useful for atomic resolution imaging of specimens that would be damaged at higher energies. However, the resolution at low voltages is degraded because of geometrical and chromatic aberrations. In the present study, we diminish the effect of these aberrations by using a delta-type corrector and a monochromator. The dominant residual aberration in a delta-type corrector, which is the sixth-order three-lobe aberration, is counterbalanced by other threefold aberrations. Defocus spread caused by chromatic aberration is reduced by using a monochromated beam with an energy spread of 0.05 eV. We obtain images of graphene and demonstrate atomic resolution at an ultralow accelerating voltage of 15 kV.

DOI: 10.1103/PhysRevLett.117.153004

Transmission electron microscopes (TEMs) are an essential tool for the analysis of the structures of materials and biological objects with high spatial resolution. After the development of aberration correctors [1], a resolution better than 0.1 nm has become accessible in the intermediate accelerating voltages of 200–300 kV [2,3]. Recently, a resolution of 45 pm was also achieved [4]. A long-standing problem in TEMs is the specimen damage caused by electron beam irradiation. One of the origins of specimen damage in TEMs is knock-on displacement, where an atom is deviated from its original structural position because of its collision with high-speed electrons. To avoid the knock-on damage, relatively low-energy electrons should be used, with energies of tens of kilo-electron-volts [5]. For example, the threshold voltage of knock-on damage for graphene is well known to be approximately 60–80 kV [6]. In the case of more damageable structures such as graphene edge atoms and fullerene molecules, the knock-on threshold voltage has been calculated to be approximately 35 kV [7]. However, such low-energy electrons cannot provide high spatial resolution. If we can record images of a damageable structure with atomic resolution at an extremely low accelerating voltage, this gentle observation technique may open the door for the analysis of specimens such as soft matter. Although a high-resolution observation has been reported at 15 kV [8], monolayer materials such as graphene have never been observed with atomic resolution. To avoid ionization damage, electrons with greater than 10 keV energy would be preferable, because the ionization cross sections of electrons below 10 keV are large [9]. Achieving atomic resolution at 15 kV is therefore an essential step to realize nondestructive observations using a TEM.

In our experiments, we have equipped a TEM with higher-order geometrical aberration correctors for the image and probe-forming lens systems. The correctors are delta type, consisting of three dodecapoles, which can correct fifth-order aberrations including sixfold astigmatism [10]. The microscope is equipped with a monochromator for the electron source. The monochromator consists of two Wien filters and a slit between the filters [11].

The correction of geometrical aberrations is a key factor in order to achieve high spatial resolution at a low accelerating voltage. Although double-hexapole-type correctors can correct geometrical aberrations including the third-order spherical aberration of an objective lens [1], aberrations higher than the third order limit the uniform phase angle to 20–35 mrad. This angle limitation is sufficient to achieve an atomic resolution of approximately 0.1 nm when the accelerating voltage is set to 80–300 kV. On the other hand, in the low accelerating voltage range of 15–60 kV, the uniform phase area limited by geometrical aberrations must be expanded to achieve a resolution equivalent to that of higher accelerating voltages. This is because of the large diffraction limit defined as $0.61\,\alpha/\lambda$, where λ is the wavelength of electron and α is the acceptance angle, which is equivalent to the flat phase angle in TEM experiments. In order to obtain a large flat phase angle, correctors that can control the fifth-order geometric aberrations have been developed [12–14]. Using these correctors, which can extend the uniform phase area to more than 40 mrad, there are reports to confirm that scanning transmission electron microscopy (STEM) can achieve atomic resolution imaging at low voltages of 60 [15] and 30 kV [16]. In the latter report, a spatial resolution of 0.11 nm has been achieved in STEM. The uniform phase angle of 40 mrad is, however, still not sufficient for atomic resolution imaging with extremely low-energy electrons of 15 keV because of the large diffraction limit caused by their long wavelength of 9.9 pm. To achieve a resolution of 0.2 nm at 15 kV, the uniform phase area must be extended

 © 2016 American Physical Society

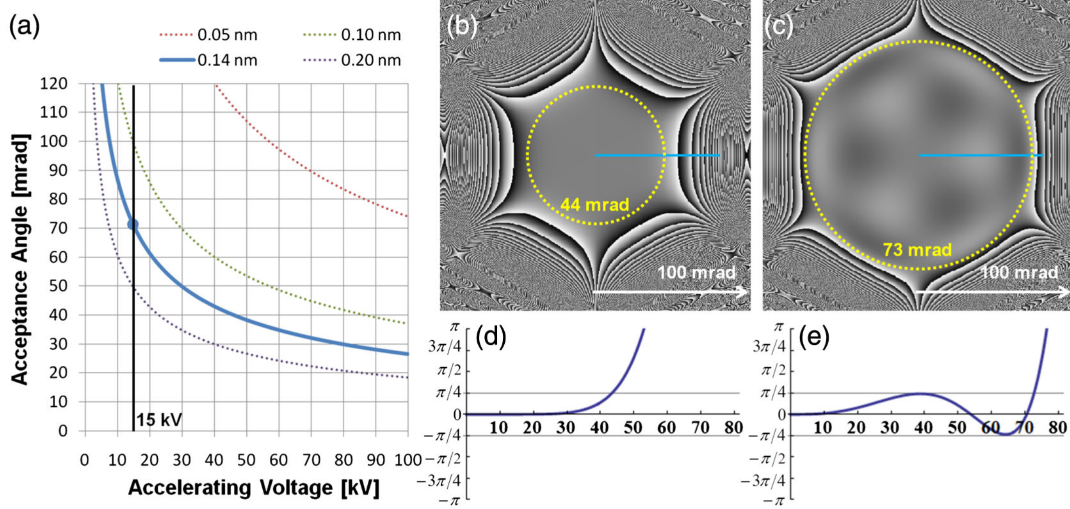

FIG. 1. (a) Acceptance angle dependence on accelerating voltage to achieve a certain resolution. Phase map of (b) $R_7 = (30\ \mathrm{mm}, 0°)$ and (c) $R_7 = (30\ \mathrm{mm}, 0°)$, $R_5 = (168\ \mu\mathrm{m}, 60°)$, $A_3 = (185\ \mathrm{nm}, 0°)$. Yellow dotted lines show $\pi/4$ limit circles. (d) and (e) show the phase plot along the blue lines in (b) and (c), respectively.

to more than 50 mrad, as shown in Fig. 1(a). In the case of a delta-type corrector [14], the dominant residual aberration is the sixth-order three-lobe aberration R_7. This aberration was measured to be approximately 30 mm, whose $\pi/4$ limit ($\alpha_{\pi/4}$) corresponds to 44 mrad, which is not sufficient to achieve atomic resolution.

To further expand the corrected angle, we counterbalanced the sixth-order three-lobe aberration R_7 with the fourth-order three-lobe aberration R_5 and the threefold astigmatism A_3, as shown in Figs. 1(b)–1(e). The situation is similar to the Scherzer defocus condition, where a positive third-order spherical aberration was counterbalanced by negative defocus. By counterbalancing the R_7 of 30 mm with an R_5 of 168 μm and an A_3 of 185 nm, the $\alpha_{\pi/4}$ expands to 73 mrad, which corresponds to a distance of less than 0.14 nm. This aberration condition can therefore provide atomic resolution images at 15 kV.

The second key factor to degrade resolution at low accelerating voltages is the defocus spread caused by chromatic aberration. The defocus spread Δ caused by chromatic aberration is expressed as $\Delta = C_c\, dE/E$, where C_c is the chromatic aberration coefficient and dE is the deviation of the electron energy E. Although the defocus spread can be affected by deviations of the accelerating voltage and lens current, they can be neglected at low accelerating voltages [17]. There are two methods to avoid resolution degradation by the chromatic aberration: First, reduce C_c by correcting the chromatic aberration of the lenses; second, reduce the energy spread of the electron source. The resolution improvement by a C_c corrector has been already demonstrated [18,19] and applied to EFTEM [20]. Resolution improvement by a monochromator has also been demonstrated at 60–300 kV [2,17,21–23]. Although TEM images have been obtained at a low voltage of 20 kV by using a C_c corrector [24] or a monochromator [25], atomic resolution has never been achieved at this voltage. In the present study, we attempted to reduce the defocus spread by using a monochromator. To increase the resolution of TEM with a monochromator, we used an imaging lens system with a small chromatic aberration coefficient of 0.6 mm at 15 kV. Figure 2(a) shows the energy width required to achieve certain resolutions at different accelerating voltages. Although the C_c generally depends on the accelerating voltage, the constant C_c of 0.6 mm is used in the calculation for simplicity. The figure indicates that an energy width of 0.2 eV, which is better than that of a cold field-emission gun, is insufficient to achieve atomic resolution at 15 kV. Figure 2(b) shows simulated images of graphene with different energy widths. The simulation indicates that the resolution strongly

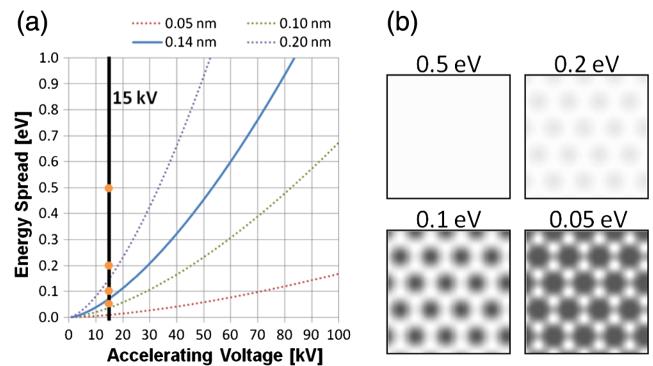

FIG. 2. (a) Energy spread (full width at half maximum) to achieve a certain resolution at each accelerating voltage. A constant C_c of 0.6 mm was used for the calculation. (b) Simulated image of graphene with different energy spreads. High-order geometrical aberrations including third- and fifth-order spherical aberrations are set to zero. Defocuses of 2.5 (0.5 and 0.2 eV), 2.0 (0.1 eV), and 1.0 nm (0.05 eV) are used in the simulation.

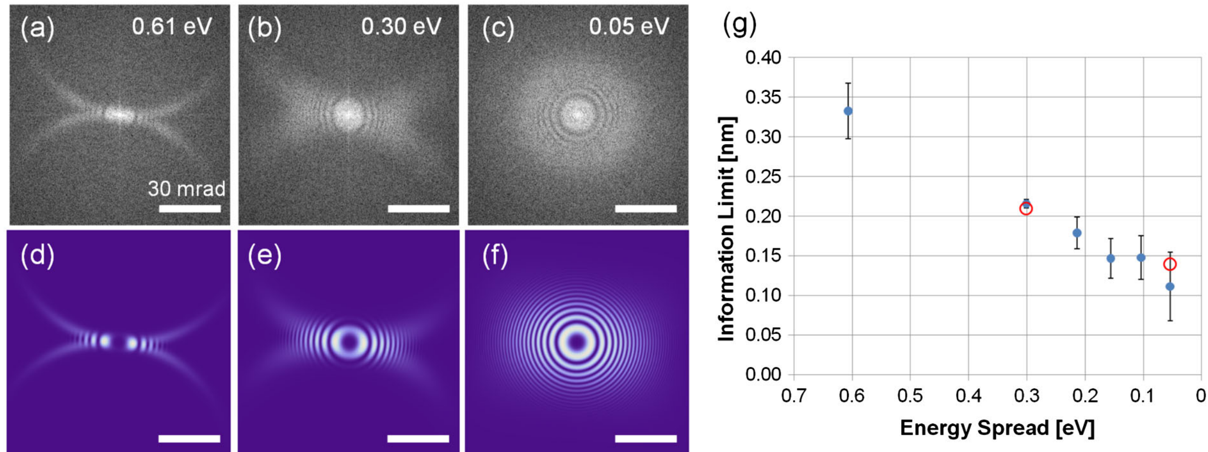

FIG. 3. Diffractograms with an illumination beam tilt of 60 mrad. The energy widths of the electron source are (a) 0.61, (b) 0.30, and (c) 0.05 eV. (d)–(f) are simulated diffractograms using an experimentally measured energy spread with a C_c of 0.6 mm. (g) Information limit of each energy spread. Blue dots show the values estimated from tilted-beam diffractograms shown in (a)–(c). Red circles show results from graphene images in Fig. 5.

depends on the energy spread, such that graphene can be imaged at atomic resolution by reducing the energy spread to 0.05 eV.

We experimentally confirmed the reduction of the defocus spread with different energy spreads using the monochromator at 15 kV. Figure 3 shows diffractograms, which are the power spectra of the Fourier transform of amorphous material TEM images. The diffractograms were recorded with an illumination beam tilt of 60 mrad. The diffractogram with a nonmonochromatic beam shown in Fig. 3(a) represents sharp achromatic circles caused by a large chromatic aberration. This diffractogram indicates that the information corresponding to the spatial frequency outside the circles is lost in the original TEM image. On the other hand, as shown in Figs. 3(b) and 3(c), the achromatic circles become thicker with narrower energy spreads. The nearly isotropic intensity of the diffractogram in Fig. 3(c) demonstrates the reduction of information transfer as the chromatic aberration is significantly improved with an energy width of 0.05 eV of the monochromatic beam. We measured the information limit of each energy spread using tilted-beam diffractograms [17,26]. Figures 3(d)–3(f) show the simulated diffractograms, and blue dots in Fig. 3(g) indicate the measured information limit. This result shows that the defocus spread and information limit can be improved drastically by reducing the energy width.

We obtained TEM images of gold nanoparticles on a carbon thin film, with different beam energy spreads, as shown in Fig. 4. No lattice fringes in the gold particles can be seen in the image with a nonmonochromatic source shown in Fig. 4(a). The lattice of atomic columns in the particles can be detected by reducing the energy width to 0.30 and 0.05 eV, as shown, respectively, in Figs. 4(b) and 4(c). The power spectra of the Fourier transform of these images show spots corresponding to a distance of 0.10 nm. The contrast caused by amorphous carbon in the diffractogram spectra increases with decreasing energy spread. These images and the spectra clearly show the resolution enhancement in the TEM images caused by narrowing the energy spread. However, it is difficult to directly quantify the resolution from Fig. 4. The high-frequency information in the power spectra is caused by the multiple-scattering electrons satisfying the achromatic condition [8]. Multiple-scattering events can have a prominent effect on the images, because lower-energy electrons have large scattering cross sections. Young's fringes may show higher-frequency information transfer than Fig. 4; they were not used here because the fringes depend on the specimen thickness. The actual resolution was expected to be lower than that displayed in Fig. 4.

The resolution in a TEM with no multiple-scattering effects was evaluated using an extremely thin specimen of monolayer graphene. Figure 5(a) shows an image of graphene obtained with a nonmonochromatic beam. Even though there was a graphene monolayer sheet in the imaged field, no graphene lattice was detected owing to the poor transfer of linear information. In the case of 0.30 eV energy spread, the image shows very weak contrast of the lattice fringes. The power spectrum shows six spots corresponding to 0.21 nm. The graphene lattice becomes detectable by reducing the energy spread. Although Fig. 4(b) shows the spots corresponding to $(0.10\ \mathrm{nm})^{-1}$, spots higher than $(0.21\ \mathrm{nm})^{-1}$ cannot be observed in Fig. 5(b). This indicates that higher spatial-frequency spots in Fig. 4(b) are caused by the effect of multiple scattering. Figure 5(c) is the image with 0.05 eV, and a magnified image is shown in Fig. 5(d). The filtered image in Fig. 5(d) was produced by the convolution of the raw image and a Gaussian function with σ of 0.04 nm. The atomic positions of graphene can be identified in the low-pass filtered image. This indicates that monolayer graphene can be imaged clearly by reducing the energy

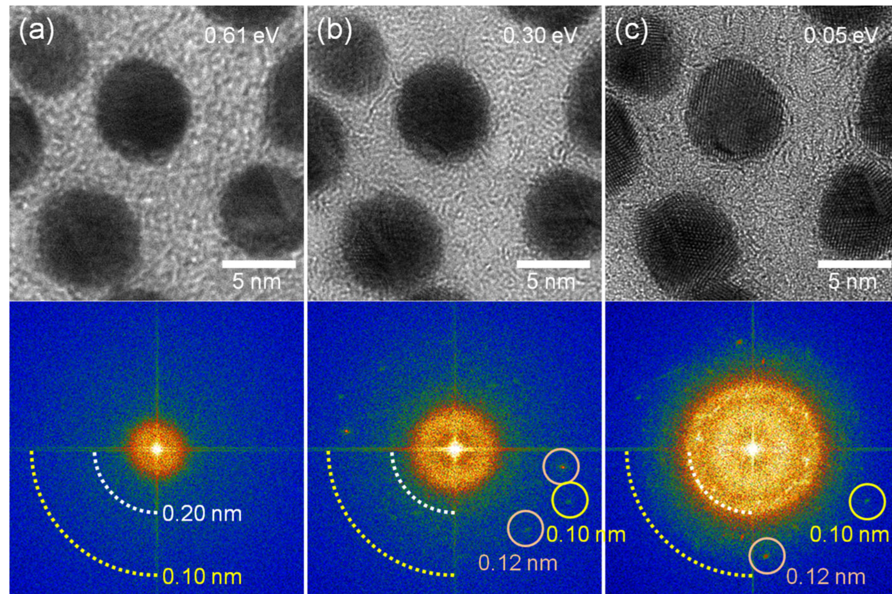

FIG. 4. TEM images of gold nanoparticles on a carbon thin film (top) and power spectra of the Fourier transform of the images (bottom). The energy widths of the electron source are (a) 0.61, (b) 0.30, and (c) 0.05 eV.

spread. The sets of spots in the power spectrum of Fig. 5(c) show that the image includes information corresponding to a distance of 0.12 nm. The distance 0.12 nm is 12 times the wavelength $\lambda = 9.9$ pm for 15 keV electrons. However, the spots are independent of the first zero in the phase contrast transfer function (PCTF) and do not support the phase relationship between the diffraction spots and the primary spot. In addition, the weak phase object approximation is not valid at 15 kV even for the monolayer graphene without multiple scattering. Thus, we determine that the resolution of the graphene image with 0.05 eV is 0.14 nm, which can be confirmed by the intensity profile of the image shown in Fig. 5(d). The ratio of the resolution to the electron wavelength reaches $d/\lambda = 14$, which has not previously been achieved in TEM or STEM. In Fig. 3(g), the red circles show the experimental results from Fig. 5. This result indicates that the monochromatic beam with an energy spread of 0.05 eV and the proposed alignment method for compensating higher-order aberration successfully enhanced the resolution.

In the TEM with the monochromator, the trade-off relationship between the energy spread and the beam current is also important. The beam current decreases with

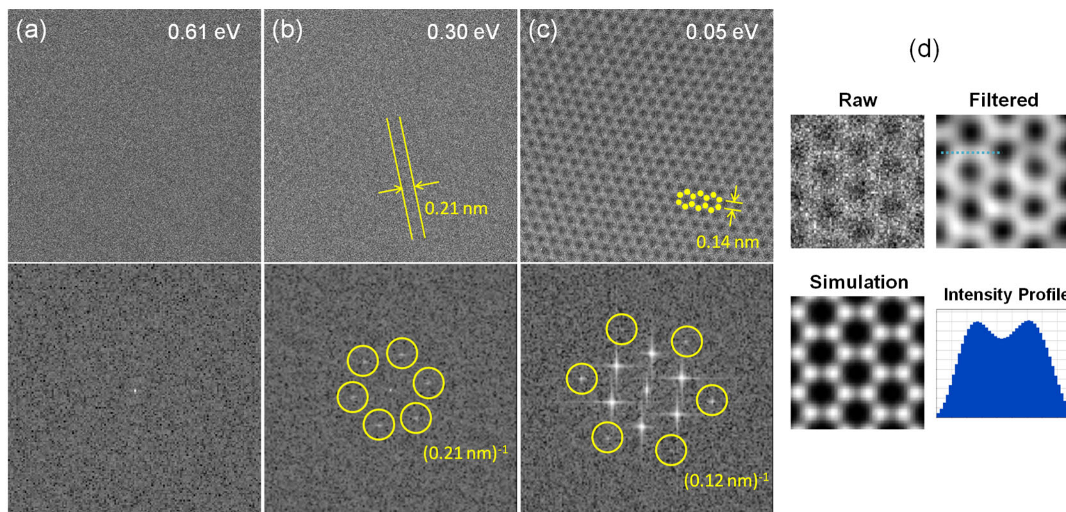

FIG. 5. Raw TEM images of monolayer graphene (top) and the power spectra of the Fourier transform of the images (bottom). The energy widths of the electron source are (a) 0.61, (b) 0.30, and (c) 0.05 eV. (d) Magnified graphene image with an energy spread of 0.05 eV. The low-pass filtered image was produced using the convolution of the Gaussian function ($\sigma = 0.04$ nm). The intensity profile along the dotted line in the filtered image is also shown. The simulation image was calculated with a C_c of 0.6 mm and a defocus of 1.0 nm.

a reduction in the energy spread. In the experiments, a beam current of 3.5 nA at 0.61 eV energy spread became 0.2 nA at 0.05 eV. To increase the signal-to-noise ratio of the images, we illuminated the small observation area with high current density. The uniform distribution of the beam energy was achieved by our use of the double Wien filter system for the monochromator. In addition, the envelope function in PCTF caused by the spatial coherence can be negligible when the high-order geometrical aberrations are corrected. The images in Fig. 5 were taken with an accumulated dose of 1×10^6 to 2×10^6 e^-/nm^2, and Fig. 5(c) was taken with an exposure time of 2 s. These values are reasonable for TEM observations. Thus, the beam current reduction in the monochromator did not become a critical issue in our experiments.

In summary, spatial resolution was improved to 0.14 nm at 15 kV by equipping a TEM with a delta-type corrector and a monochromator. The power spectrum of monolayer graphene image showed spots corresponding to 0.12 nm. The acceptance angle for an objective lens was further expanded by counterbalancing the sixth-order three-lobe aberration with the fourth-order three-lobe aberration and the threefold astigmatism. The resolution degradation by chromatic aberration was evaluated by the reduced energy spread of the electron source. We demonstrated an observation of a monolayer graphene at atomic resolution by TEM with an energy width of 0.05 eV at 15 kV. The low-voltage TEM using the monochromator will be useful for the analyses of various beam-sensitive materials.

The authors thank S. Sasaki and the engineers at JEOL who contributed to this work for their cooperation towards development and installation of the microscope. This work was supported by the JST (Japan Science and Technology Agency) under the Research Acceleration Program (2012–2016).

*shmorish@jeol.co.jp

[1] M. Haider, S. Uhlemann, E. Schwan, H. Rose, B. Kabius, and K. Urban, Nature (London) **392**, 768 (1998).
[2] C. Kisielowski *et al.*, Microsc. Microanal. **14**, 469 (2008).
[3] R. Erni, M. D. Rossell, C. Kisielowski, and U. Dahmen, Phys. Rev. Lett. **102**, 096101 (2009).
[4] H. Sawada, N. Shimura, F. Hosokawa, N. Shibata, and Y. Ikuhara, Microscopy **64**, 213 (2015).
[5] R. F. Egerton, R. McLeod, F. Wang, and M. Malac, Ultramicroscopy **110**, 991 (2010).
[6] J. C. Meyer, F. Eder, S. Kurasch, V. Skakalova, J. Kotakoski, H. J. Park, S. Roth, A. Chuvilin, S. Eyhusen, G. Benner, A. V. Krasheninnikov, and U. Kaiser, Phys. Rev. Lett. **108**, 196102 (2012).
[7] K. Suenaga, Y. Iizumi, and T. Okazaki, Eur. Phys. J. Appl. Phys. **54**, 33508 (2011).
[8] T. Sasaki, H. Sawada, F. Hosokawa, Y. Sato, and K. Suenaga, Ultramicroscopy **145**, 50 (2014).
[9] S. P. Khare, M. K. Sharma, and S. Tomar, J. Phys. B **32**, 3147 (1999).
[10] H. Sawada, T. Sasaki, F. Hosokawa, S. Yuasa, M. Terao, M. Kawazoe, T. Nakamichi, T. Kaneyama, Y. Kondo, K. Kimoto, and K. Suenaga, Ultramicroscopy **110**, 958 (2010).
[11] M. Mukai, J. S. Kim, K. Omoto, H. Sawada, A. Kimura, A. Ikeda, J. Zhou, T. Kaneyama, N. P. Young, J. H. Warner, P. D. Nellist, and A. I. Kirkland, Ultramicroscopy **140**, 37 (2014).
[12] H. Müller, S. Uhlemann, P. Hartel, and M. Haider, Microsc. Microanal. **12**, 442 (2006).
[13] O. L. Krivanek, G. J. Corbin, N. Dellby, B. F. Elston, R. J. Keyse, M. F. Murfitt, C. S. Own, Z. S. Szilagyi, and J. W. Woodruff, Ultramicroscopy **108**, 179 (2008).
[14] H. Sawada, T. Sasaki, F. Hosokawa, S. Yuasa, M. Terao, M. Kawazoe, T. Nakamichi, T. Kaneyama, Y. Kondo, K. Kimoto, and K. Suenaga, J. Electron Microsc. **58**, 341 (2009).
[15] O. L. Krivanek, M. F. Chisholm, V. Nicolosi, T. J. P ennycook, G. J. Corbin, N. Dellby, M. F. Murfitt, C. S. Own, Z. S. Szilagyi, M. P. Oxley, S. T. Pantelides, and S. J. Pennycook, Nature (London) **464**, 571 (2010).
[16] H. Sawada, T. Sasaki, F. Hosokawa, and K. Suenaga, Phys. Rev. Lett. **114**, 166102 (2015).
[17] S. Morishita, M. Mukai, K. Suenaga, and H. Sawada, Appl. Phys. Lett. **108**, 013107 (2016).
[18] B. Kabius, P. Hartel, M. Haider, H. Müller, S. Uhlemann, U. Loebau, J. Zach, and H. Rose, J. Electron Microsc. **58**, 147 (2009).
[19] M. Haider, P. Hartel, H. Müller, S. Uhlemann, and J. Zach, Microsc. Microanal. **16**, 393 (2010).
[20] K. W. Urban, J. Mayer, J. R. Jinschek, M. J. Neish, N. R. Lugg, and L. J. Allen, Phys. Rev. Lett. **110**, 185507 (2013).
[21] B. Freitag, S. Kujawa, P. M. Mul, J. Ringnalda, and P. C. Tiemeijer, Ultramicroscopy **102**, 209 (2005).
[22] P. C. Tiemeijer, M. Bischoff, B. Freitag, and C. Kisielowski, Ultramicroscopy **114**, 72 (2012).
[23] J. H. Warner, E. R. Margine, M. Mukai, A. W. Robertson, F. Giustino, and A. I. Kirkland, Science **337**, 209 (2012).
[24] P. Ercius, M. Boese, T. Duden, and U. Dahmen, Microsc. Microanal. **18**, 676 (2012).
[25] U. Kaiser, J. Biskupek, J. C. Meyer, J. Leschner, L. Lechner, H. Rose, M. Stoger-Pollach, A. N. Khlobystov, P. Hartel, H. Muller, M. Haider, S. Eyhusen, and G. Benner, Ultramicroscopy **111**, 1239 (2011).
[26] J. Barthel and A. Thust, Phys. Rev. Lett. **101**, 200801 (2008).